**Supplement**

# Rapid formation of secondary aerosol precursors from the autoxidation of $C_5$–$C_8$ *n*-aldehydes

Shawon Barua[1,*], Avinash Kumar[1], Prasenjit Seal[1], Siddharth Iyer[1], and Matti Rissanen[1,2,*]

[1]Aerosol Physics Laboratory, Physics Unit, Faculty of Engineering and Natural Sciences, Tampere University, 33720 Tampere, Finland

[2]Department of Chemistry, University of Helsinki, 00560 Helsinki, Finland

*Correspondence to: shawon.barua@tuni.fi, matti.rissanen@tuni.fi

## S1. Flow reactor setup

A schematic of the flow reactor setup used in *n*-aldehyde OH oxidation reactions is shown in Figure S1. All the reactant gas supply lines were connected to the reactor via PTFE tubing and Swagelok fittings. The gas flows were controlled by Alicat mass flow controllers (MFC). The mass spectrometer chemical ionization inlet flow (8–10 slpm) and the volume of the reactor defines the reaction time of the gas mixture inside the reactor. A 100 cm long borosilicate flow reactor with 4.7 cm inner diameter (i.d.) was used for long reaction time experiments while a quartz flow reactor (length: 100 cm, and i.d.: 2.2 cm) was used for the short reaction time experiments. Short reaction time experiments were achieved by providing the precursor VOC flow via a movable injector tube within the reactor and adjusting the distance of the injector tip with respect to the mass spectrometer orifice. The deuterated water ($D_2O$) line and the NO line were connected separately only during the hydrogen to deuterium (H/D) exchange experiment and the oxidation experiment in presence of NO, respectively.

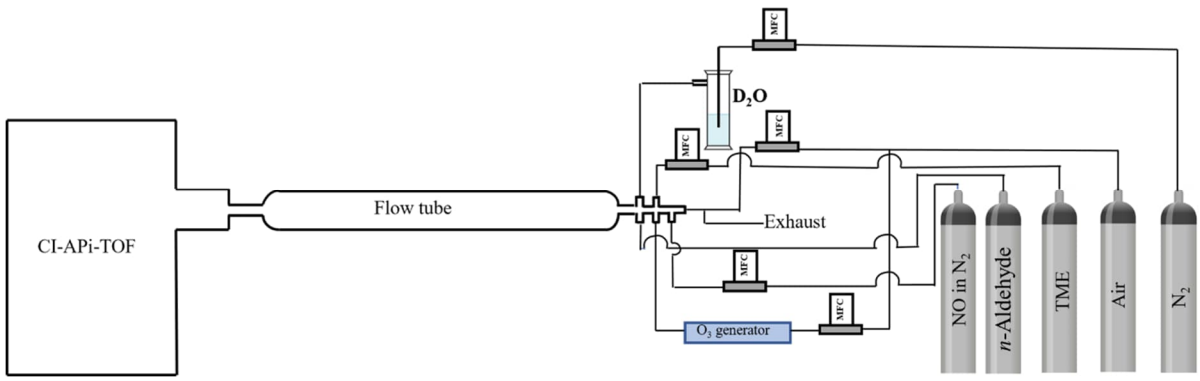


Figure S1. A nitrate ($NO_3^-$) based chemical ionization mass spectrometer coupled to ambient pressure flow reactor. TME = tetramethylethylene ($C_6H_{12}$). The oxidant OH radical was produced in situ by TME + $O_3$ reaction.

The mass spectrometric data processing, including averaging, mass axis calibration, and peak integration, was done using the tofTools v6.03 package for MATLAB. The signal intensities of all the detected species were normalized using the following expression:

$$S = \frac{[X_i * NO_3^-]}{[NO_3^-] + [HNO_3NO_3^-] + [(HNO_3)_2NO_3^-]}$$

where $[X_i * NO_3^-]$ represents the intensity of an individual species corresponding to $i^{th}$ mass/charge.

## S2. Chemicals

High purity Nitrogen gas (5.0 grade) was obtained from Woikoski and Linde Oy. The NO gas cylinder (100 ppm in $N_2$) was obtained from Advanced Speciality gases. Deuterium oxide (99.9 atom % D) was obtained from Sigma Aldrich and was transferred to the flow reactor by bubbling nitrogen gas through a liquid $D_2O$ reservoir. The following chemicals were used to make individual gas cylinders diluted in $N_2$: Tetramethylethylene (98%), hexanal (98%), heptanal (Supelco, purity ≥ 97.0%), and octanal (99%) all from Sigma Aldrich while pentanal (97%) was obtained from Acros Organics. All the chemicals were used without further purification.

## S3. *n*-Heptanal ozonolysis background

In the OH initiated oxidation experiment of *n*-heptanal, we used exceptionally low precursor concentrations compared to other studied *n*-aldehydes (see Table 1 in the main manuscript). This was done to reduce the *n*-heptanal ozonolysis background signals originating from unknown contaminants from the heptanal cylinder. The ozonolysis background signals with high and low precursor conditions are shown in Figure S2. Under low precursor condition, we avoid the interference of these background signals with the heptanal OH oxidation products. Figure S2 clearly shows that the heptanal ozonolysis background signals are distinct from the heptanal OH oxidation product signals, $C_7H_{12}O_4$ (m/z 222), $C_7H_{12-14}O_5$ (m/z 238–240), $C_7H_{12-14}O_6$ (m/z 254–256), $C_7H_{12-14}O_7$ (m/z 270–272), $C_7H_{12-14}O_8$ (m/z 286–288), $C_{14}H_{26}O_9$ (m/z 400), $C_{14}H_{26}O_{10}$ (m/z 416), and $C_{14}H_{26}O_{11}$ (m/z 432) that are shown in Figure 2 in the main manuscript.

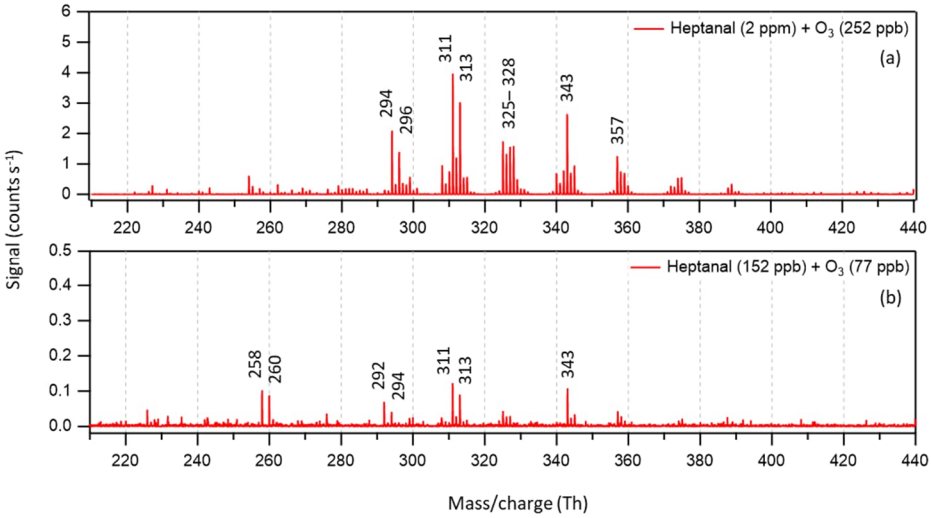


Figure S2. Heptanal + ozone background spectra measured with different reactant concentrations: high (a), and low (b). The unidentified products likely originate from a heptanal stabilizer added by the chemical supplier. Note: Heptanal oxidation experiment initiated by OH radicals (see Figure 2 in the main manuscript) was conducted using the same concentrations of heptanal and ozone as condition (b) and with the addition of TME (as the source of OH).

## S4. Autoxidation an aldehyde – hexanal

The oxidation reaction of an aldehyde by OH radical is initiated predominantly by the abstraction of the aldehydic hydrogen on C1. The H abstraction can also take place on other carbons (e.g., C4) distant from the aldehydic moiety (see Figure S3 below adapted from Barua et al. (2023)). Both reaction channels produce a carbon centred radical that can add molecular oxygen atoms and form acyl (or alkyl) peroxy radicals ($RC(O)O_2$ or $RO_2$) which can subsequently autoxidize to form highly oxygenated organic molecules (HOMs). Figure S3 shows that the autoxidation of hexanal along C1 and C4 channels with initial branching of 86 % and 8 %, respectively, produce the same $O_5$ $RO_2$ (A61) as the dominant reaction intermediate. The A61 radical slowly turns over to $O_7$ $RO_2$ (A61a) via subsequent reactions along the autoxidation path. The other *n*-aldehydes (e.g., pentanal–octanal) are likely to undergo similar autoxidation mechanism and form HOMs we observed experimentally as shown in the main manuscript.

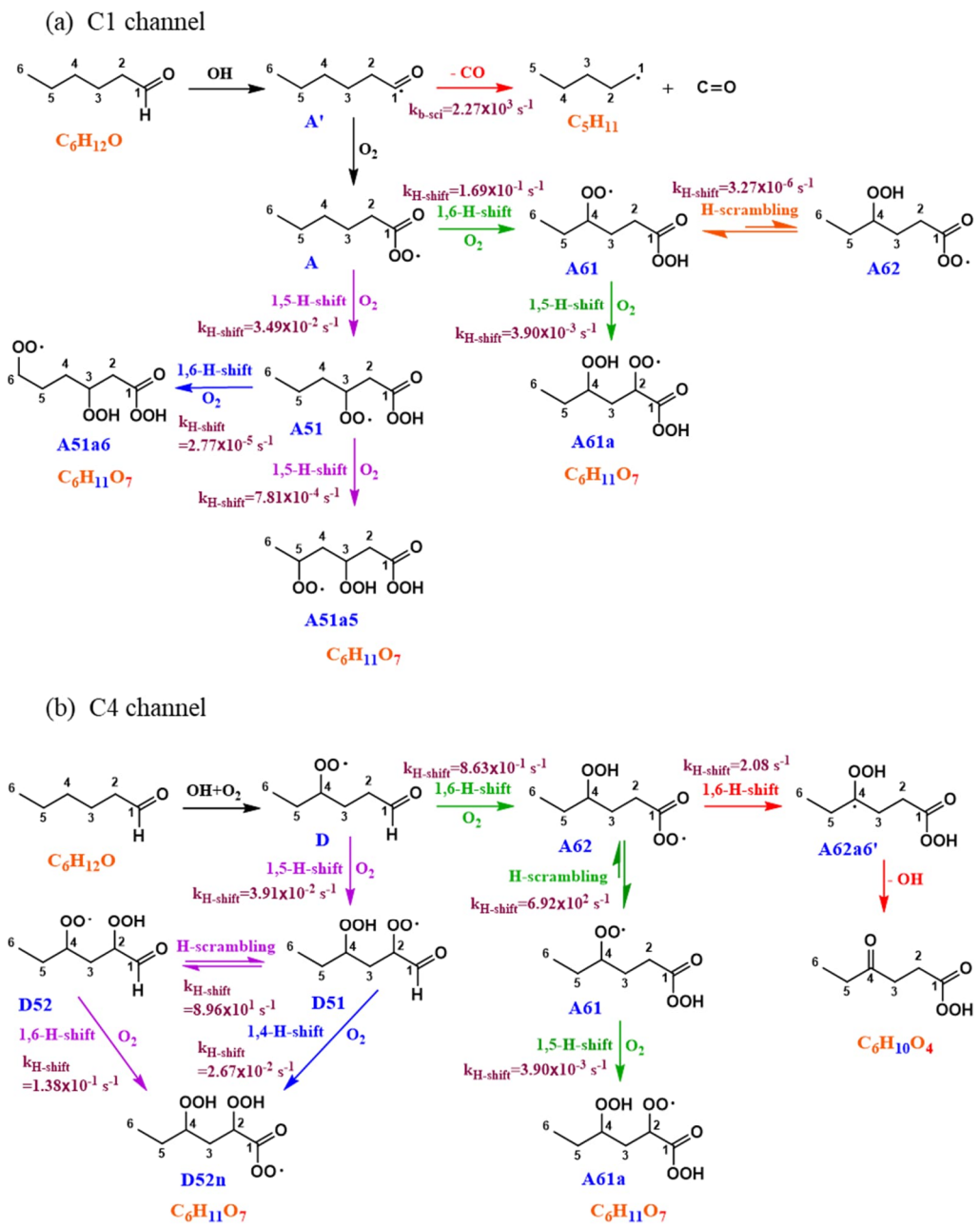


Figure S3. Autoxidation mechanism of hexanal + OH reaction initiated by H atom abstraction from the aldehydic carbon (a) and from a non-aldehydic carbon (b) forming $O_7$ HOM shown by Barua et al. (2023). Along the dominant aldehydic H abstraction channel (branching ratio 86 %), the formation of $O_5$ product (A61) is very fast and the subsequent H-shift reaction is relatively slower. The non-aldehydic H abstraction channel (branching ratio 8 %) shows a slower production of $O_5$ product (D52) compared to A61, which subsequently undergoes a fast H-shift reaction.

## S5. Autoxidation forming $O_9$ HOM in *n*-aldehydes

With the increase of carbon chain length in the studied *n*-aldehyde oxidation experiments, we observed the formation of more oxygenated products with up to a $O_9$ monomeric HOM in the case of octanal. In Figure S4, the autoxidation mechanism originated from hexanal work (see Figure S3 above) is extended to HOM up to 9 oxygen atoms. The autoxidation generated radical intermediates ($C_nH_{2n-1}O_{7,9}$) can also undergo chain termination reactions forming closed-shell products via OH loss, via Russell mechanism forming an alcohol and a carbonyl species (red arrows in Figure S4), and H abstraction from $HO_2$ radicals ($RO_2 + HO_2 \rightarrow ROOH + O_2$).

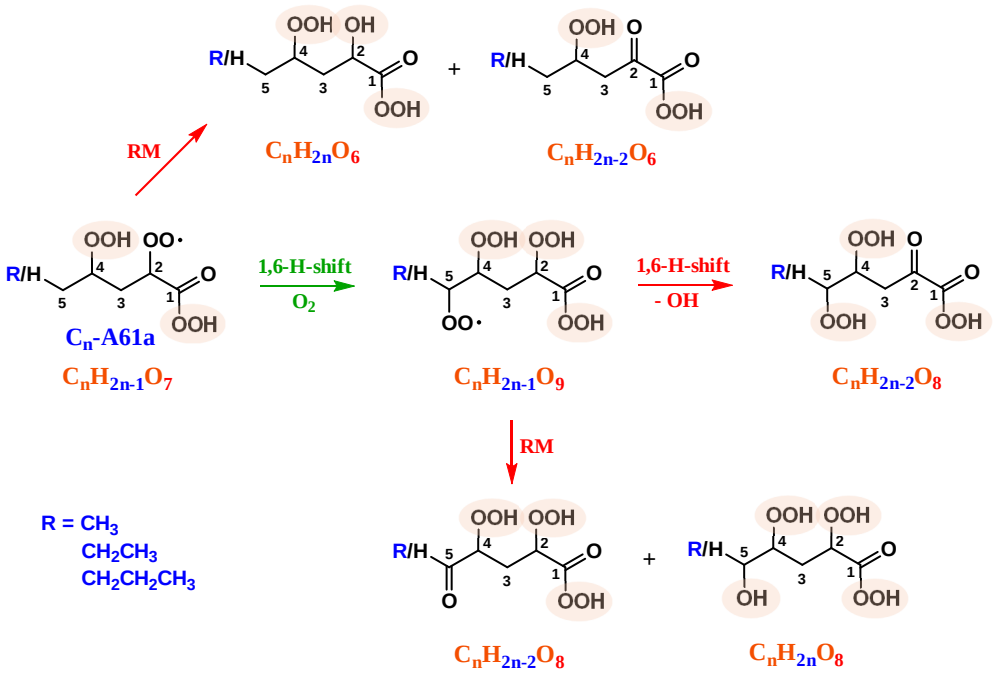


Figure S4. Autoxidation mechanism of *n*-aldehyde + OH reaction extended from Figure S3 showing the formation of HOM up to $O_9$ (green arrow) along with reaction chain termination products (red arrows). RM = Russell mechanism ($RO_2 + R'O_2 \rightarrow ROH + R'_{-H}C{=}O + O_2$).

## S6. Bimolecular reaction products

This section describes potential reaction mechanisms leading to the identified products which involve one $RO_2$ bimolecular reaction step forming alkoxy radical (RO) intermediates ($RO_2 + RO_2 \rightarrow 2\ RO + O_2$). While considering H-shift reactions in the alkoxy radicals ($C_nH_{2n-1}O_4$), progressively longer H-shift span (from 1,4 H-shift in $C_5H_9O_4$ to 1,6 H-shift in $C_8H_{15}O_4$, see Figures S5–S8) becomes more relevant (Vereecken and Peeters, 2010) as the carbon chain length of the precursor aldehyde increases. The alkoxy radical can also undergo H-scrambling reaction with the peroxy acid group (Yang et al., 2024) forming hydroxyl acylperoxy radical (see Figure S9 below). These mechanisms show the most probable formation paths of dominant

$O_6$ alkyl peroxy radicals ($C_nH_{2n-1}O_6$) we observed in the studied $C_5$–$C_8$ *n*-aldehyde oxidation during short reaction time experiments (see Figure 1 in the main manuscript). In the case of heptanal and octanal in Figures S7–S8, we show the reaction chain propagation forming $C_nH_{2n-1}O_8$ radicals (green arrows) that we observed experimentally (see Figure 2 in the main manuscript). Besides, the likely formation of the closed-shell $O_5$ and $O_6$ products originating from $C_nH_{2n-1}O_6$ radicals are also shown in Figures S5–S9. In the molecular structures, the labile hydrogen containing groups are marked in light-brown shapes. The structures associated with the proposed mechanisms are in agreement with the hydrogen to deuterium (H to D) exchange experiments (see Figure 6 in the main manuscript).

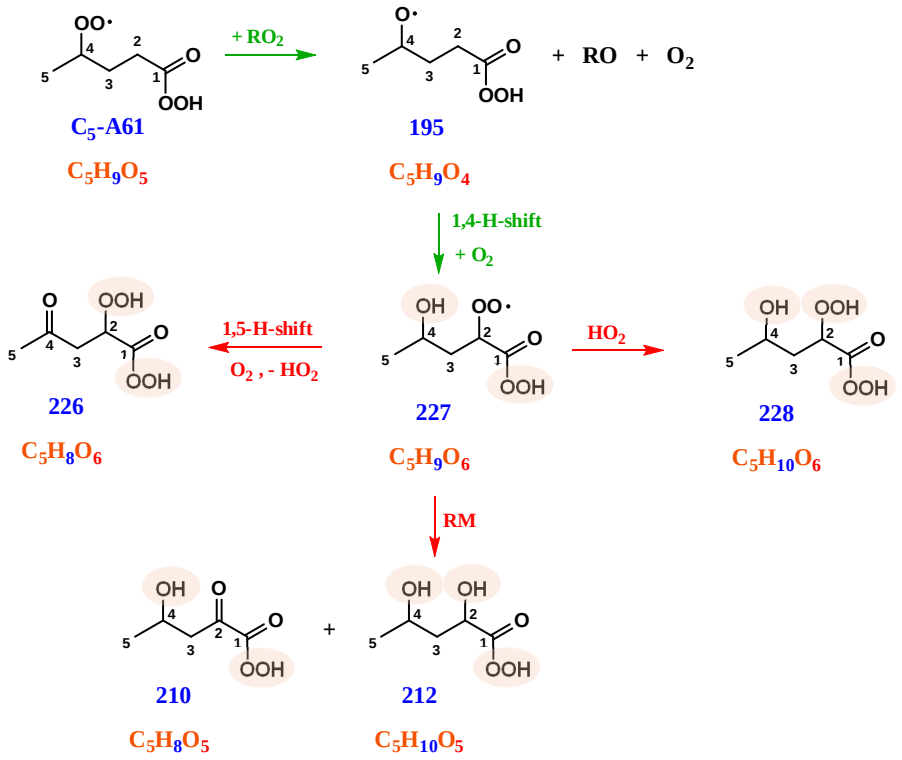


Figure S5. Formation of $C_5H_{8-10}O_6$ products in pentanal + OH reaction likely involve $C_5$-A61 ($C_5H_9O_5$) peroxy radical undergoing bimolecular reactions with other peroxy radicals ($RO_2$). The $C_5H_9O_6$ (nominal mass 227) radical likely undergo Russell mechanism (RM: $RO_2$ + $R'O_2$ → ROH + $R'_{-H}C{=}O$ + $O_2$) forming closed-shell $O_5$ products.

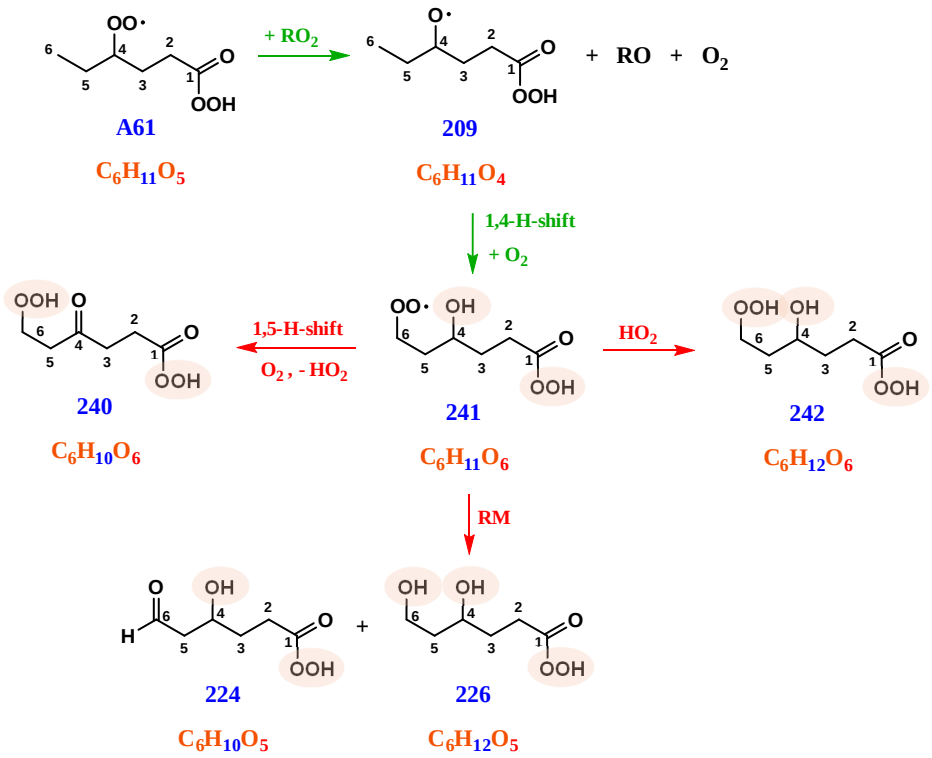


Figure S6. Formation of $C_6H_{10–12}O_6$ products in hexanal + OH reaction likely involve A61 ($C_6H_{11}O_5$) peroxy radical undergoing bimolecular reactions with other peroxy radicals ($RO_2$). The $C_6H_{11}O_6$ (nominal mass 241) radical likely undergo Russell mechanism (RM: $RO_2$ + $R'O_2$ → ROH + $R'_{-H}C{=}O$ + $O_2$) forming closed-shell $O_5$ products.

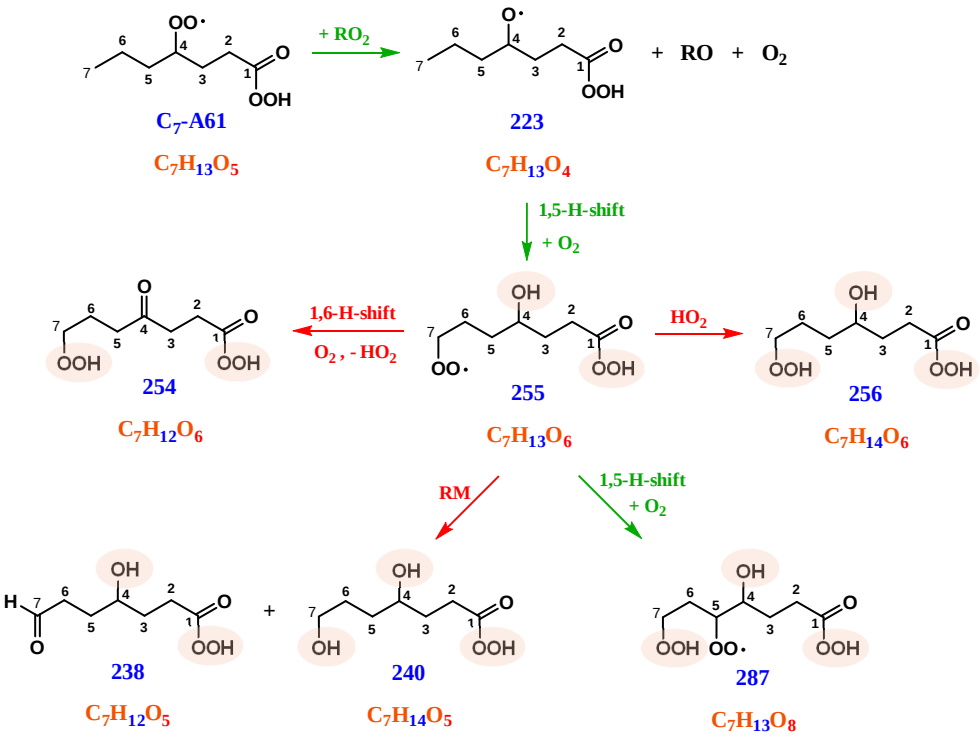

Figure S7. Formation of $C_7H_{12-14}O_6$ products in heptanal + OH reaction likely involve $C_7$-A61 ($C_7H_{13}O_5$) peroxy radical undergoing bimolecular reactions with other peroxy radicals ($RO_2$). The $C_7H_{13}O_6$ (nominal mass 255) radical can propagate autoxidation forming $C_7H_{13}O_8$ (nominal mass 287) radical (green arrow). It can also undergo Russell mechanism (RM: $RO_2$ + $R'O_2$ → ROH + $R'_{-H}C{=}O$ + $O_2$) forming closed-shell $O_5$ products.

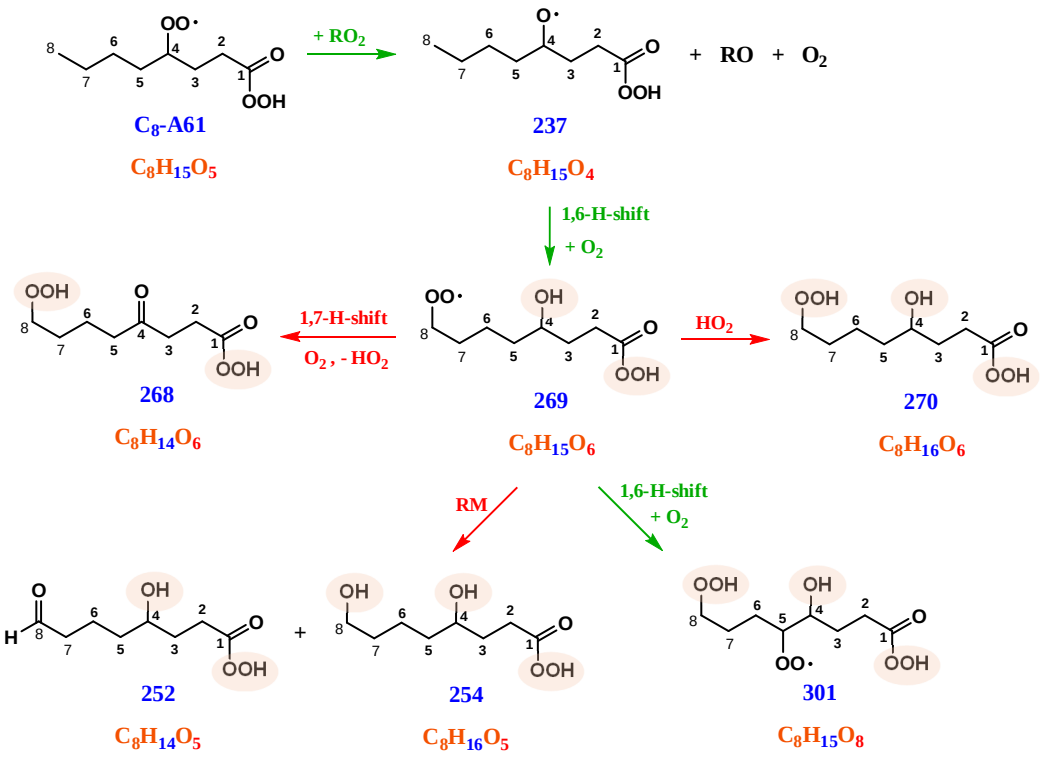


Figure S8. Formation of $C_8H_{14-16}O_6$ products in octanal + OH reaction likely involve $C_8$-A61 ($C_8H_{15}O_5$) peroxy radical undergoing bimolecular reactions with other peroxy radicals ($RO_2$). The $C_8H_{15}O_6$ (nominal mass 269) radical can propagate autoxidation forming $C_8H_{15}O_8$ (nominal mass 301) radical (green arrow). It can also undergo Russell mechanism (RM: $RO_2$ + $R'O_2$ → ROH + $R'_{-H}C{=}O$ + $O_2$) forming closed-shell $O_5$ products.

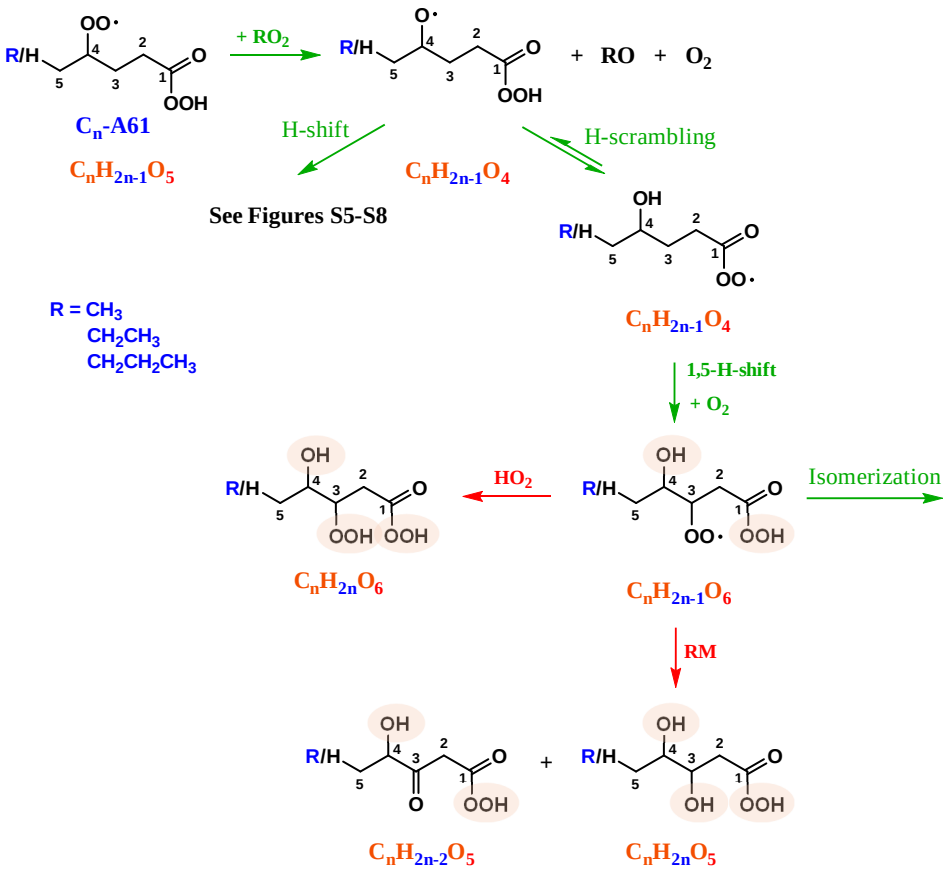


Figure S9. Formation of $C_nH_{2n-1}O_6$ peroxy radical in *n*-aldehyde + OH reaction involving H-scrambling reaction of an alkoxy radical intermediate $C_nH_{2n-1}O_4$ originating from $C_n$-A61 ($C_nH_{2n-1}O_5$) peroxy radical via bimolecular reactions with other peroxy radicals ($RO_2$). The $O_6$ $RO_2$ radical can propagate autoxidation via isomerization channel (green arrow). It can also react with $HO_2$ and undergo Russell mechanism (RM: $RO_2 + R'O_2 \rightarrow ROH + R'_{-H}C{=}O + O_2$) forming closed-shell $O_6$ and $O_5$ products, respectively.

## S7. HOM accretion products ($C_{2n}H_{4n-2}O_{9-11}$)

In the OH initiated *n*-aldehyde oxidation experiments, we observed the formation of HOM accretion products according to a general reaction $RO_2 + R'O_2 \rightarrow ROOR' + O_2$ (Hasan et al., 2020; Valiev et al., 2019; Bianchi et al., 2019). The reactions forming the accretion products ($C_{16}H_{30}O_{9-11}$) in octanal oxidation are shown in Figure S10 which involve self and cross reactions of alkyl peroxy radicals ($C_8H_{15}O_{5-7}$). Note that the molecular structures shown here do not represent their exact spatial orientation but provide the number of available functional groups. In the studied $C_5$–$C_8$ *n*-aldehyde systems, the reactant $RO_2$ radicals ($C_nH_{2n-1}O_{5-7}$) with same number of O atoms have identical number(s) of OH, OOH, and C(O)OOH groups according to Figures S4–S9. The corresponding accretion products ($C_{2n}H_{4n-2}O_{9-11}$) will have an equivalent number of OH, OOH, and C(O)OOH groups as shown here for octanal, marked

in light-brown shapes (see Figure S10). These are in agreement with the $D_2O$ mediated H to D shifts (see Figure 6 in the main manuscript).

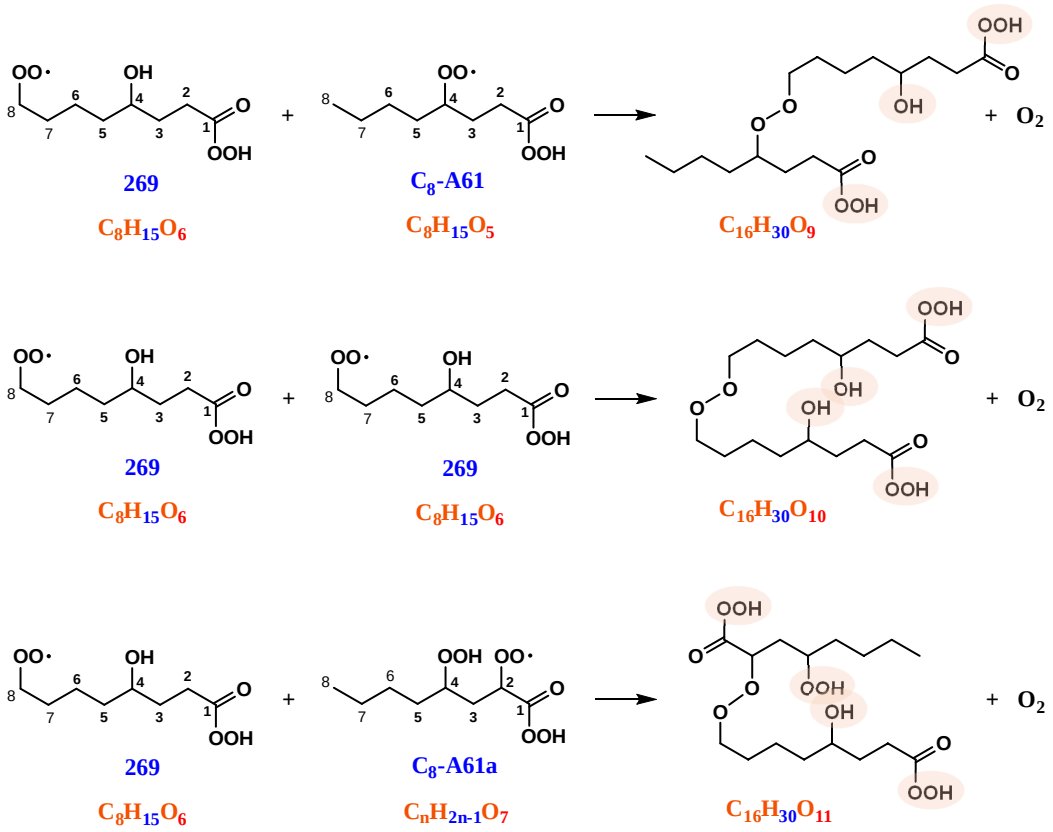


Figure S10. Formation of HOM accretion products ($C_{16}H_{30}O_{9\text{-}11}$) in octanal + OH reaction via alkyl peroxy self and cross reactions ($RO_2 + R'O_2 \rightarrow ROOR' + O_2$). Similar reactions apply for other *n*-aldehyde systems involving $C_nH_{2n\text{-}1}O_{5\text{–}7}$ $RO_2$ radicals to produce corresponding accretion products ($C_{2n}H_{4n\text{-}2}O_{9\text{–}11}$) with equivalent number of OH, OOH, and C(O)OOH groups.

## S8. TME-derived accretion products

In our *n*-aldehyde oxidation experiments, the oxidant OH radicals were produced in situ by the ozonolysis reaction of tetramethylethylene (TME) (see Figure S11). The reaction leads to the formation of a keto peroxy radical ($C_3H_5O_3$) and acetone ($CH_3COCH_3$) along with OH radicals. The TME-derived peroxy radical $C_3H_5O_3$ can react with aldehyde-derived peroxy radicals $C_nH_{2n\text{-}1}O_{6\text{–}8}$ and form different accretion products ($C_{n+3}H_{2n+4}O_{7\text{–}9}$) as shown in Figure 2 in the main manuscript. One example of such reactions involving hexanal-derived peroxy radical $C_6H_{11}O_6$ is shown in Figure S11.

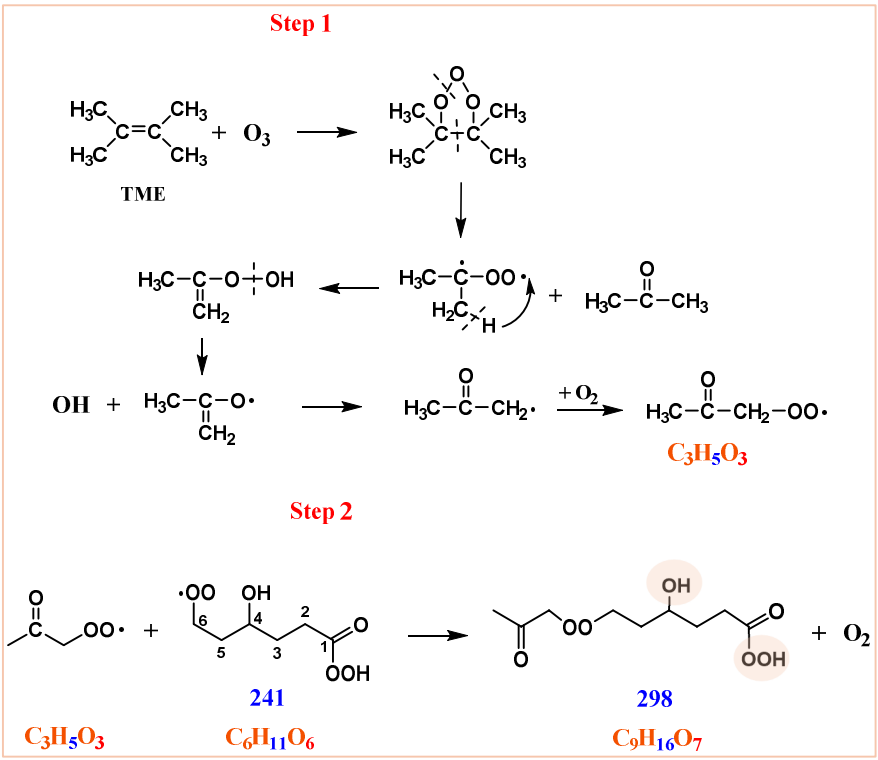


Figure S11. Production of oxidant OH in tetramethylethylene (TME) ozonolysis. The keto peroxy radical $C_3H_5O_3$ is a biproduct and reacts with aldehyde-derived peroxy radicals $C_n$ $RO_2$ yielding accretion products with $C_{n+3}$ atoms; a pathway producing $C_9H_{16}O_7$ accretion product in hexanal oxidation is shown as an example.

## S9. $D_2O$ experiments

During the *n*-aldehyde OH oxidation experiments in presence of $D_2O$, a near complete H/D exchange was achieved which is most conveniently monitored from the reagent ions, from the shift of $HNO_3NO_3^-$ and $(HNO_3)_2NO_3^-$signals by one and two mass unit, respectively on the mass spectrum (see Figure S12).

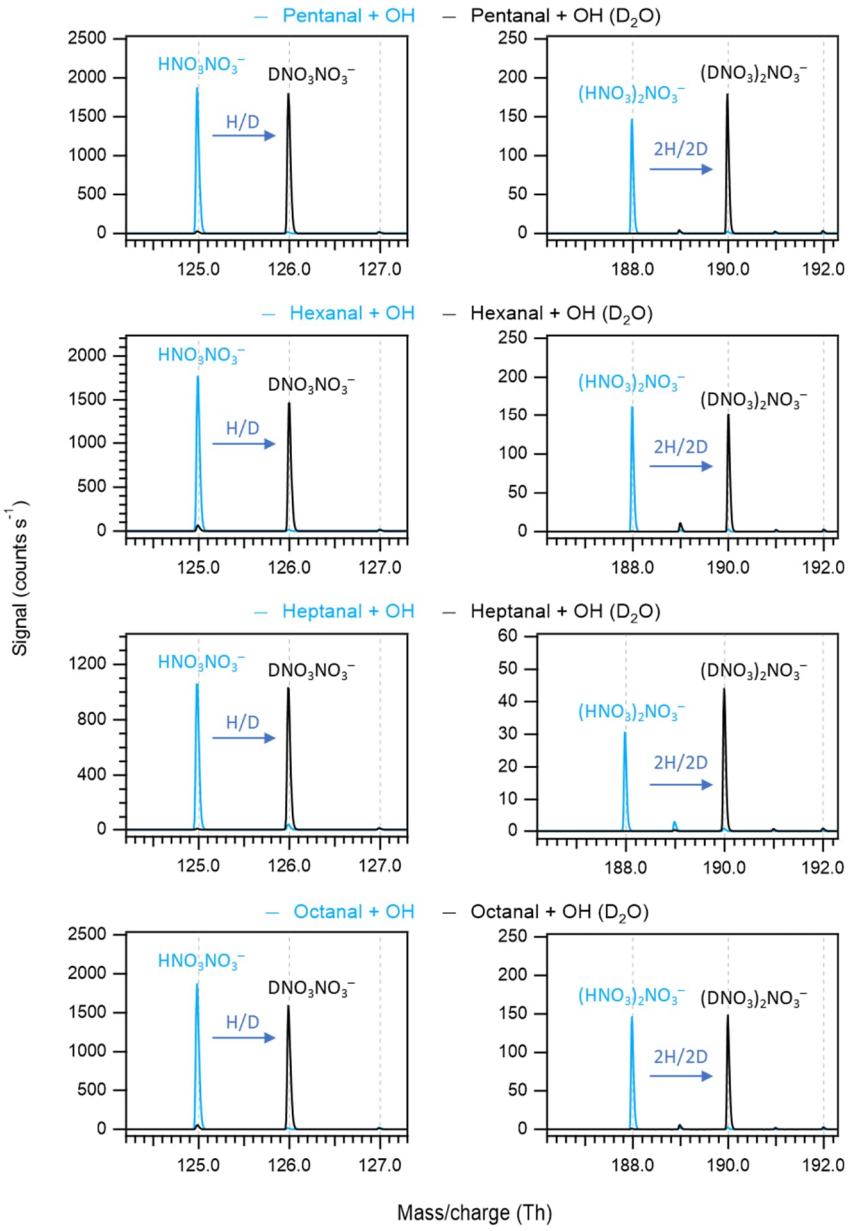


Figure S12. H/D exchange in the reagent ions $HNO_3NO_3^-$ and $(HNO_3)_2NO_3^-$ converting them into $DNO_3NO_3^-$ and $(DNO_3)_2NO_3^-$, respectively, during different *n*-aldehyde OH oxidation reaction in presence of $D_2O$.

## References

Barua, S., Iyer, S., Kumar, A., Seal, P., & Rissanen, M. (2023). An aldehyde as a rapid source of secondary aerosol precursors: Theoretical and experimental study of hexanal autoxidation. *Atmospheric Chemistry and Physics*, *23*(18), 10517–10532. https://doi.org/10.5194/acp-23-10517-2023

Bianchi, F., Kurtén, T., Riva, M., Mohr, C., Rissanen, M. P., Roldin, P., Berndt, T., Crounse, J. D., Wennberg, P. O., Mentel, T. F., Wildt, J., Junninen, H., Jokinen, T., Kulmala, M., Worsnop, D. R., Thornton, J. A., Donahue, N., Kjaergaard, H. G., & Ehn, M. (2019). Highly Oxygenated Organic Molecules (HOM) from Gas-Phase Autoxidation Involving Peroxy Radicals: A Key Contributor to Atmospheric Aerosol. *Chemical Reviews*, *119*(6), 3472–3509. https://doi.org/10.1021/acs.chemrev.8b00395

Hasan, G., Salo, V.-T., Valiev, R. R., Kubečka, J., & Kurtén, T. (2020). Comparing Reaction Routes for$^3$ (RO⋯OR′) Intermediates Formed in Peroxy Radical Self- and Cross-Reactions. *The Journal of Physical Chemistry A*, *124*(40), 8305–8320. https://doi.org/10.1021/acs.jpca.0c05960

Valiev, R. R., Hasan, G., Salo, V.-T., Kubečka, J., & Kurten, T. (2019). Intersystem Crossings Drive Atmospheric Gas-Phase Dimer Formation. *The Journal of Physical Chemistry A*, *123*(30), 6596–6604. https://doi.org/10.1021/acs.jpca.9b02559

Vereecken, L., & Peeters, J. (2010). A structure–activity relationship for the rate coefficient of H-migration in substituted alkoxy radicals. *Physical Chemistry Chemical Physics*, *12*(39), 12608. https://doi.org/10.1039/c0cp00387e

Yang, X., Wang, H., Lu, K., Ma, X., Tan, Z., Long, B., Chen, X., Li, C., Zhai, T., Li, Y., Qu, K., Xia, Y., Zhang, Y., Li, X., Chen, S., Dong, H., Zeng, L., & Zhang, Y. (2024). Reactive aldehyde chemistry explains the missing source of hydroxyl radicals. *Nature Communications*, *15*(1), 1648. https://doi.org/10.1038/s41467-024-45885-w